

1

2

3

4 **Title: Intra-genome variability in the dinucleotide composition of SARS-CoV-2**

5 Paul Digard¹, Hui Min Lee¹, Colin Sharp¹, Finn Grey¹, Eleanor Gaunt^{1*}

6 ¹The Roslin Institute, The University of Edinburgh, Easter Bush Campus, Midlothian, EH25 9RG,
7 UK

8 *corresponding author: Elly.Gaunt@ed.ac.uk

9 Abstract

10 CpG dinucleotides are under-represented in the genomes of single stranded RNA viruses, and
11 coronaviruses, including SARS-CoV-2, are no exception to this. Artificial modification of CpG
12 frequency is a valid approach for live attenuated vaccine development, and if this is to be applied to
13 SARS-CoV-2, we must first understand the role CpG motifs play in regulating SARS-CoV-2
14 replication. Accordingly, the CpG composition of the newly emerged SARS-CoV-2 genome was
15 characterised in the context of other coronaviruses. CpG suppression amongst coronaviruses does not
16 significantly differ according to genera of virus, but does vary according to host species and primary
17 replication site (a proxy for tissue tropism), supporting the hypothesis that viral CpG content may
18 influence cross-species transmission. Although SARS-CoV-2 exhibits overall strong CpG
19 suppression, this varies considerably across the genome, and the Envelope (E) open reading frame
20 (ORF) and ORF10 demonstrate an absence of CpG suppression. While ORF10 is only present in the
21 genomes of a subset of coronaviruses, E is essential for virus replication. Across the *Coronaviridae*, E
22 genes display remarkably high variation in CpG composition, with those of SARS and SARS-CoV-2
23 having much higher CpG content than other coronaviruses isolated from humans. Phylogeny indicates
24 that this is an ancestrally-derived trait reflecting their origin in bats, rather than something selected for
25 after zoonotic transfer. Conservation of CpG motifs in these regions suggests that they have a
26 functionality which over-rides the need to suppress CpG; an observation relevant to future strategies
27 towards a rationally attenuated SARS-CoV-2 vaccine.

28

29 Introduction

30 CpG dinucleotides are under-represented in the DNA genomes of vertebrates (Cooper and Krawczak
31 1989; Simmonds, et al. 2013). Cytosines in the CpG conformation may become methylated, and this
32 methylation is used as a mechanism for transcriptional regulation (Medvedeva, et al. 2014).
33 Methylated cytosines have a propensity to undergo spontaneous deamination (and so conversion to a
34 thymine). Over evolutionary time, this has reduced the frequency of CpGs in vertebrate genomes
35 (Cooper and Krawczak 1989). However, loss of CpGs in promoter regions would affect
36 transcriptional regulation, and so CpGs are locally retained, resulting in functionally important ‘CpG
37 islands’ found in around half of all vertebrate promoter regions (Deaton and Bird 2011).

38 Single strand RNA (ssRNA) viruses infecting vertebrate hosts reflect the CpG dinucleotide
39 composition of their host in a type of mimicry (Simmonds, et al. 2013). It was hypothesised that this
40 is because vertebrates have evolved a CpG sensor which flags transcripts with aberrant CpG
41 frequencies (Atkinson, et al. 2014; Gaunt, et al. 2016). This idea was strengthened by the discovery
42 that the cellular protein Zinc-finger Antiviral Protein (ZAP) binds CpG motifs on viral RNA and
43 directs them for degradation (Takata, et al. 2017), and further supported by observations that CpGs
44 can be synonymously introduced into a viral genome to the detriment of virus replication without
45 negatively impacting transcriptional or translational efficiency (Tulloch, et al. 2014; Gaunt, et al.
46 2016). Current understanding is therefore that ssRNA viruses mimic the CpG composition of their
47 host at least in part to subvert detection by ZAP. ssRNA viruses also under-represent the UpA
48 dinucleotide, but to a far more modest extent (Simmonds, et al. 2013), and the reasons behind UpA
49 suppression are less well understood. A consequence of dinucleotide bias is that certain codon pairs
50 are under-represented (Tulloch, et al. 2014; Kunec and Osterrieder 2016) (so, for example, codon
51 pairs of the conformation NNC-GNN are among the most rarely seen codon pairs in vertebrates (Tats,
52 et al. 2008)). Whether the two phenomena of CpG suppression and codon pair bias (CPB) are discrete
53 remains controversial (Futcher, et al. 2015; Kunec and Osterrieder 2016; Groenke, et al. 2020).

54 The *Coronaviridae* have a generally low genomic cytosine content (Berkhout and van Hemert 2015),
55 but as with other ssRNA viruses, nonetheless still under-represent CpG dinucleotides to a frequency
56 below that predicted from individual base frequencies of cytosine and guanine (Woo, et al. 2007).

57 The Coronavirus family comprises four genera – the alpha, beta, gamma and delta-coronaviruses.
58 Human-infecting coronaviruses (HCoVs) have been identified belonging to the alpha and beta genera
59 (Hu, et al. 2015). Alphacoronaviruses infecting humans include HCoV-229E and the more recently
60 discovered HCoV-NL63 (van der Hoek, et al. 2004). Betacoronaviruses include HCoV-OC43, HCoV-
61 HKU1 (Woo, et al. 2005), severe acute respiratory syndrome (SARS)-CoV (Rota, et al. 2003), Middle
62 East respiratory syndrome (MERS)-CoV (Zaki, et al. 2012) and the recently emerged SARS-CoV-2
63 (Lu, et al. 2020; Zhu, et al. 2020). Prior to the emergence of SARS-CoV-2, SARS-CoV had the
64 strongest CpG suppression across human-infecting coronaviruses (Woo, et al. 2007). The reason(s)
65 for this are uncertain, but loss of CpG from a virus genome upon zoonotic transfer into the human
66 host has previously been reported for influenza A virus (Greenbaum, et al. 2008), potentially
67 indicating an advantage of reduced CpG content for infection of the human respiratory tract. All
68 human-infecting coronaviruses are thought to be derived from ancestral bat viruses, though
69 intermediate hosts may have facilitated zoonotic passage in some cases (Banerjee, et al. 2019).

70 During replication, coronaviruses synthesise transcriptionally active negative sense sub-genomic
71 RNAs which are of varying length. Sub-genomic RNAs are synthesised by the viral polymerase
72 copying the genome up to a 5' leader sequence (Liao and Lai 1994) which is repeated upstream of
73 most open reading frames (ORFs) in the coronavirus genome (such repeats are referred to as
74 transcription regulation sequences (TRSs)); this complementarity allows viral polymerase jumping
75 from the 5' leader sequence to directly upstream of ORFs preceded by a TRS (Sawicki and Sawicki
76 1998). The negative sense sub-genomic RNAs serve as efficient templates for production of mRNAs
77 (Sawicki, et al. 2007). Generally, only the first ORF of a sub-genomic mRNA is translated (Perlman
78 and Netland 2009), although leaky ribosomal scanning has been reported as a means for accessing
79 alternative ORFs for several coronaviruses including SARS-CoV (Schaecher, et al. 2007).

80 SARS-CoV-2 was recently reported to have a CpG composition lower than other members of the
81 betacoronavirus genus, comparable to certain canine alphacoronaviruses; an observation used to draw
82 inferences over its origin and/or epizootic potential (Xia 2020). Here we show that coronaviruses have
83 a broad range of CpG composition which is partially host and tissue tropism dependent, and that there
84 is no difference in CpG content across coronavirus genera. There is however a striking disparity in
85 CpG composition between SARS-CoV-2 ORFs, with the Envelope (E) protein ORF and ORF10 over-
86 representing CpG dramatically. E ORF and ORF10 also have higher UpA dinucleotide composition
87 and lower CPB scores than other ORFs. E ORF displays CpG suppression in all human-infecting
88 viruses except SARS-CoV and SARS-CoV-2, suggesting a potential correlation between CpG
89 presentation and disease severity in human-infecting coronaviruses.

90

91 Results

92 **CpG suppression within coronavirus genomes varies between host species and tissue tropism**
93 **but not between genera.** The genomic CpG composition of all complete genome coronavirus
94 sequences ($n = 3407$; downloaded and further processed as described in the methods section and **Fig**
95 **1**) were calculated using observed: expected (O:E) ratios, with any value below 1 indicating CpGs are
96 under-represented relative to the genomic content of cytosine and guanine bases. A substantial range
97 in GC content (from $\sim 0.32 - 0.47$) was seen across the *Coronaviridae*, and as expected, all viruses
98 exhibited some degree of CpG suppression, with CpG O:E ratios ranging from 0.37 to 0.74 (**Fig 2A**).
99 To investigate the root of this variation, the coronavirus sequence dataset was refined to remove
100 sequences with more than 90% nucleotide identity to reduce sampling biases (so, for example, SARS-

101 CoV sequences of human origin were stripped from over 1000 representative sequences to just one).
102 The CpG compositions of the remaining 215 sequences (**Table S1**) were compared between
103 coronavirus genera (alpha, beta, gamma and delta). For the 215 representative sequences, a genus
104 could be assigned for 203. No differences in CpG composition between coronavirus genera were
105 apparent, although the gamma genus exhibited a tighter range (**Fig 2B**). Next, we examined whether
106 differences in CpG composition between viruses isolated from different hosts explained the range in
107 CpG composition across the *Coronaviridae*. For the 215 representative sequences, a host could be
108 assigned to 210. Coronavirus sequences were divided into host groups, and groups with at least three
109 divergent sequences were compared; this included bat, avian, camelid, canine, feline, human,
110 mustelid, rodent, swine and ungulate viruses. Variation in CpG composition between coronaviruses
111 detected in different host species was evident across groups ($p = 0.0057$) and between groups, with
112 coronaviruses detected in canine and human species having lower CpG content and rodent and bat
113 coronaviruses having the highest (**Fig. 2C**). Significant differences in CpG composition were detected
114 between bat and canine ($p = 0.0001$), avian and rodent ($p = 0.005$), canine and mustelid ($p = 0.011$),
115 canine and rodent ($p < 0.0001$), human and rodent ($p = 0.002$), and rodent and ungulate ($p = 0.0026$)
116 viruses. All frequency ranges overlapped however, indicating viral CpG frequency alone seems to be
117 a poor predictor of virus origin, contradicting the recent suggestion of a canine origin of SARS-CoV-2
118 (Xia 2020). Where sequences in a host group representative of both alpha and betacoronaviruses were
119 available (which was the case for bat, camelid, canine, human, rodent and swine viruses), these
120 sequences were split by genus and compared to determine whether coronavirus genera influenced
121 coronavirus CpG frequencies in a host species-specific manner. By this method, the lack of difference
122 in CpG composition of coronaviruses of different genera was maintained (**Fig. 2D**).

123 To test the hypothesis that coronavirus CpG content varies according to tissue tropism (Xia 2020), we
124 classified the viruses according to their primary site of replication, where this was known or could be
125 inferred from the sampling route. Samples were split into five categories – ‘respiratory’, ‘enteric’,
126 ‘multiple’, ‘other’, or ‘unknown’. Altogether, 206 of the 215 sequences were classifiable (detailed in
127 **Table S1**), with 9 sequences categorised as ‘unknown’ and excluded from further analyses. By this
128 admittedly inexact approach, viruses infecting the respiratory tract had a significantly lower mean
129 CpG composition than viruses with enteric tropism ($p = 0.032$; **Fig. 2E**). However, the spread of
130 respiratory virus CpG frequencies was contained entirely within the range exhibited by enteric
131 viruses. Furthermore, 124 sequences were assigned to the enteric group, and only 22 to the respiratory
132 group. Of these 146 sequences, bat viruses accounted for 80, all of which were assigned to the enteric
133 group (despite reasonable sampling of respiratory tract in bats) and this cohort of viruses maintained
134 almost the full spread of CpG frequencies (**Fig. 2E, Table S1**). Thus, while coronavirus CpG
135 frequency may show some correlation with replication site, the dataset available does not permit
136 strong conclusions to be drawn or predictions about zoonotic potential to be made.

137 **Heterogeneities in the dinucleotide composition of SARS-CoV-2.** By our methods for calculating
138 CpG O:E ratios, SARS-CoV-2 has a genomic CpG ratio of 0.408 (representing the mean of 1163
139 complete genome sequences). This is similar to the value calculated previously for a much smaller
140 sample ($n = 5$) of SARS-CoV-2 sequences (Xia 2020). As this previous study noted, this is at the
141 bottom end of the range of genomic CpG O:E ratios for betacoronaviruses and for coronaviruses
142 detected in humans (**Figs 2B, C and D**). However, as noted above, vertebrate DNA genomes contain
143 localised islands of higher CpG content (Deaton and Bird 2011). To determine if similar
144 heterogeneity in CpG frequency was evident in the SARS-CoV-2 genome, the composition of
145 individual ORFs was examined. Overall, most ORFs had CpG O:E ratios which were comparable to
146 the genomic CpG ratio. However, two ORFs in particular, E ORF and ORF10, had CpG ratios higher
147 than 1, indicating an absence of CpG suppression in those regions (**Fig. 3A**). These two ORFs also did
148 not suppress the UpA dinucleotide, in contrast with other SARS-CoV-2 ORFs (**Fig. 3B**).

149 Due to the difficulties in distinguishing between dinucleotide bias and CPB, CPB scores were also
150 calculated for each ORF and plotted against CpG composition (**Fig. 3C**). CPB scores provide an
151 indication of whether the codon pairs encoded in each ORF are congruous with usage in vertebrate
152 genomes. A score below 0 indicates use of codon pairs that are disfavoured in host ORFs. An
153 approximately linear relationship between CpG O:E ratio and CPB score for each SARS-CoV-2 ORF
154 was apparent ($R^2 = 0.80$). E ORF and ORF10 both had negative CPB scores, indicating that they use
155 under-represented codon pairs and in keeping with the observation that both ORFs over-represent
156 CpG and UpA dinucleotides.

157 To examine the precise location of the CpG hotspots, a sliding window analysis of CpG content
158 across the 3' end of the SARS-CoV-2 genome (averaged over 1163 complete genome sequences) as
159 well as the closely related bat and pangolin sequences was performed. As expected, marked increases
160 in CpG O:E ratio were observed concomitant with the genomic regions associated with E ORF and
161 ORF10 (**Fig. 3D**). The E ORF and ORF10 regions associated with high CpG composition were
162 maintained across the bat, pangolin and human sequences, indicating that since the bat sample was
163 collected in 2013, the higher CpG frequency in this region has not been negatively selected. While the
164 increase in CpG presentation was apparent across the entire E ORF, starting at the 3' end of ORF3
165 and ending at the beginning of the M gene, the CpG spike in ORF10 was more narrowly associated
166 with the putative coding region. Additionally, a CpG spike between the 3'-end of ORF8 and the 5'-
167 end of the N gene was evident. The 5'-end of the N ORF also contains the overlapping ORF9b gene,
168 which when considered alone, has a CpG O:E ratio approaching 1 (**Fig. 3A**), and is the ORF with the
169 third-highest CpG O:E ratio after E ORF and ORF10. The usual coding plasticity afforded to
170 nucleotides in the third position of a codon is nullified when overlapping reading frames are present,
171 and so the CpG spike at this gene boundary is not surprising. Thus, although the SARS-CoV-2
172 genome exhibits high CpG suppression overall, there are local heterogeneities associated with
173 individual ORFs, most notably E.

174 **On the origins of the high CpG content of E ORF of SARS-CoV-2.** To determine whether the high
175 CpG content of E ORF is evolutionarily conserved (ORF10 is poorly conserved and only encoded by
176 a subset of SARS-like coronaviruses, so it was not analysed), attempts to identify the E ORF by
177 nucleotide alignment for the set of 215 coronavirus sequences was undertaken, compared with E
178 ORFs already annotated in NCBI. Of the 215 sequences, E ORF was identifiable in 178, with the
179 remaining sequences too divergent to be confident of gene assignment. CpG composition for E ORF
180 for the 178 sequences was measured and plotted according to host (**Fig. 4A**). A diverse distribution of
181 CpG content was evident in viruses from every host group except ungulates, with bats in particular
182 displaying a notable range from total suppression to overrepresentation. Otherwise, most viruses from
183 most species still maintained some level of CpG suppression in E ORF. Overall, there was a
184 significant difference between the mean CpG O:E ratio across host groups by 1-way ANOVA ($p <$
185 0.0001), but no significant differences were identified in pairwise comparisons of viral CpG
186 compositions between hosts. The exceptions with high CpG O:E ratios in E ORF were four avian
187 coronaviruses and notably, SARS-CoV and SARS-CoV-2. In contrast, other human-infecting
188 coronaviruses (HCoV-229E, HCoV-HKU1, HCoV-NL63 and HCoV-OC43) all strongly under-
189 represented CpG in E ORF, while MERS-CoV E ORF had an intermediate CpG O:E ratio of 0.6. To
190 confirm E ORF over-represented CpG relative to the rest of the genome in SARS-CoV and SARS-
191 CoV-2, ratios for E ORF: genomic CpG O:E were calculated (**Fig. 4B**). In non-bat non-avian host
192 genomes, E ORF usually displayed CpG suppression in line with or stronger than that seen at the
193 genome level, whereas SARS-CoV and SARS-CoV-2 starkly contrasted with this, displaying far less
194 CpG suppression in this region.

195 To investigate the evolutionary history of E ORF CpG composition in the human-infecting
196 coronaviruses, a phylogenetic reconstruction of all 7 human coronavirus and 96 bat coronavirus E
197 genes was performed to determine whether CpG ratios in this region were ancestrally derived. As

198 expected (Cotten, et al. 2013; Lu, et al. 2020), the human viruses were interspersed among the bat
199 viruses, reflective of their independent emergence events (**Fig. 4C**). The CpG compositions of the
200 human coronavirus E ORFs, although diverse, were similar to the CpG compositions of their nearest
201 bat relatives, demonstrating that CpG composition in E ORF is an ancestrally derived trait selected
202 prior to emergence in the human population.

203

204 **Discussion**

205 We have examined the CpG O:E ratios of all the currently available complete genome sequences of
206 coronaviruses and uncovered a noteworthy diversity. Generally, the CpG O:E ratio of coronavirus
207 genomes from a single host species varied considerably. For bats, which serve as a coronavirus
208 reservoir (Banerjee, et al. 2019) and which had the largest number of representative sequences, the
209 CpG O:E range was from 0.41 to 0.70, demonstrating the genome plasticity of coronaviruses and
210 indicating that their evolution is not overtly restricted by a requirement to minimise CpG composition
211 in the natural reservoir. The antiviral CpG-detector protein, ZAP (Takata, et al. 2017), has been
212 identified as a target for several viral proteins including the 3C protease of enterovirus 71 (Xie, et al.
213 2018) and NS1 of influenza A virus (Tang, et al. 2017) – two viruses with overall low CpG content
214 (Atkinson, et al. 2014; Gaunt, et al. 2016). This highlights the importance of CpG as a pathogen-
215 associated molecular pattern (PAMP), and so this diversity in CpG expression within the
216 *Coronaviridae* is striking. If coronaviruses also produce a protein with anti-ZAP activity, it is possible
217 that this has variable efficacy between strains, explaining the ability of coronaviruses to fluctuate CpG
218 composition considerably. Alternatively (or in addition), this may be host driven; we show that
219 average CpG suppression varies with host species (**Fig 2C**) and, as previously suggested (Xia 2020),
220 this may be linked with ZAP expression levels. We have demonstrated that CpG variation is not
221 related to viral taxonomic grouping (**Fig. 2B**) but we did find an association between viral CpG
222 composition and primary replication site, with respiratory coronaviruses having a lower CpG
223 composition than enteric ones (**Fig. 2E**). This is the opposite of what has been previously suggested
224 (Xia 2020), though this proposal was not supported by any comprehensive investigation.
225 Nevertheless, our meta-analysis was subject to the sampling preferences of many labs who have
226 performed surveillance for coronaviruses, and many of the tissue tropism assignments we made have
227 not been verified by experimental infections. Another limitation of this analysis is that only sequences
228 of greater than 10% divergence were included. Tissue tropism can be defined by much smaller
229 differences; for example, a deletion in the spike protein of transmissible gastroenteritis virus (a
230 porcine coronavirus) altered the tropism of the virus from enteric to respiratory, while nucleotide
231 identity was preserved at 96% (Cox, et al. 1990; Rasschaert, et al. 1990). Further study on tissue
232 tropisms of coronaviruses, as well as tissue expression profiles and antiviral activities of ZAP are
233 needed to validate these analyses.

234 Loss of CpG motifs during adaptation to the human host has been previously described for influenza
235 A virus (Greenbaum, et al. 2008), highlighting the importance of CpG composition for host
236 adaptation. For SARS-CoV-2, we determined a genomic CpG O:E ratio of 0.408, which is similar to
237 the human genome CpG O:E ratio of 0.2-0.4 (McClelland and Ivarie 1982; Sved and Bird 1990;
238 Tomso and Bell 2003). Mimicry of the CpG composition of the host by ssRNA viruses is considered a
239 mechanism to subvert detection by the innate immune response (Simmonds, et al. 2013; Takata, et al.
240 2017) and speculatively this may indicate that SARS-CoV-2 was genetically predisposed to make a
241 host switch into humans. Similarly, the genomic CPB score of 0.048 indicates that SARS-CoV-2 uses
242 codon pairs which are preferentially utilised in the human ORFeome, which may mean that the virus
243 was well suited for translational efficiency in humans at its time of emergence.

244 In coding regions which do not have overlapping ORFs, there is no requirement at the coding level for
245 CpG motifs to be retained (Kanaya, et al. 2001). E ORF and ORF10 are not known to be in

246 overlapping reading frames; conversely, ORF9b overlaps with the ORF for nucleocapsid (N). Some
247 CpG retention in this region is therefore inevitable and may explain the high CpG composition of
248 ORF9b. This nevertheless leaves open the question of why CpG motifs are retained in the E ORF and
249 ORF10 regions (if this is not an ancestrally derived evolutionary hangover; as CpGs have not been
250 lost from these regions between 2013 and now (**Fig. 3D**), this seems unlikely). CpG motifs may serve
251 various non-exclusive purposes, including providing secondary structure (Rima and McFerran 1997),
252 intentionally stimulating ZAP activity (by analogy with multiple viruses intentionally triggering NF-
253 kB (Hiscott, et al. 2001)), or providing m5c methylation sites (Squires, et al. 2012; Khoddami and
254 Cairns 2013; Dev, et al. 2017).

255 It is also possible that CpG enrichment serves as a strategy for regulating translation. Conceivably, the
256 high CpG content at the 5' end of the E ORF transcript destines this for degradation via ZAP or CBP-
257 associated mechanisms (Guo, et al. 2007; Groenke, et al. 2020) more rapidly than other viral
258 transcripts. This could be intentional, or an evolutionarily accepted trade-off to preserve a higher
259 importance role for CpGs. Alternatively, E ORF and ORF10 proteins may only be required late during
260 infection (parallels with which can be drawn from the differential temporal expression and
261 translational efficiencies of transcripts of the coronavirus mouse hepatitis virus strain A59 (Irigoyen,
262 et al. 2016)), by which time an as-yet unidentified inhibitor of ZAP (or other CpG/CBP sensor(s))
263 may render CpG suppression unnecessary, as suggested for human cytomegalovirus (Lin, et al. 2020).

264 ORF9b and ORF10 do not have their own TRSs and so whether or how these open reading frames are
265 accessed is currently controversial; nevertheless, peptides from both have been identified by mass
266 spectrometry from SARS-CoV-2 infected cells (Davidson, et al. 2020). The ORF9b AUG
267 transcription initiation site, which has a strong Kozak context (Kozak 1986), is the first AUG after
268 and 10 nucleotides downstream of the initiation site for N ORF (which displays moderate Kozak
269 context). It is therefore credible to think that ORF9b is accessed via leaky ribosomal scanning - a well
270 characterised method for accessing alternative ORFs used by coronaviruses and other viruses (Lin and
271 Lo 1992; Chenik, et al. 1995; Schneider, et al. 1997; Senanayake and Brian 1997; O'Connor and Brian
272 2000; Ryabova, et al. 2006; Firth and Atkins 2010; Wise, et al. 2011; Irigoyen, et al. 2016). There is a
273 lack of evidence that ORF10 is accessed via production of its own subgenomic RNA (Kim, et al.
274 2020); possibly, this ORF is accessed via leaky scanning from the leader immediately preceding the N
275 ORF. However, visual inspection of the SARS-CoV-2 genome indicated that the AUG encoding
276 ORF10 is 24 AUGs downstream from the one initiating N ORF, making this hypothesis speculative at
277 best. Whether the anomalous CpG composition of ORF10 is somehow involved in priming its
278 transcription remains to be determined.

279 The transcript encoding E ORF incorporates an additional ~3.4kb of RNA and ORF10, if accessed
280 from the transcript produced from the TRS upstream of N ORF, is present on a transcript of
281 approximately 1.6kb in length. Whether the described CpG enriched regions are relevant as PAMPs in
282 these contexts is currently unclear from what is known about ZAP recognition of CpG motifs. It is
283 also worth noting that the body TRS sequence ahead of the E gene is relatively weak in SARS-CoV-2,
284 as it is in SARS-CoV (Marra, et al. 2003), suggesting that this subgenomic mRNA may be of
285 relatively low abundance. Of the SARS-CoV-2 transcripts which use a canonical TRS for synthesis,
286 the donor site upstream of E ranked seventh when comparing sequencing read frequency across this
287 site (behind reads spanning the TRS sites upstream of N, spike, ORF7a, ORF7b, ORF3a, ORF8 and
288 M ORF respectively) in Vero cells infected at a low MOI for 24 hours, indicating that E ORF is of
289 lower abundance than most other transcripts (Kim, et al. 2020). It is therefore possible that E ORF is
290 of sufficiently low abundance for a high CpG frequency to be physiologically inconsequential.
291 Similar logic can be applied to ORF10, which is just 117 nucleotides in length.

292 Synonymous addition of CpGs into a virus genome has been suggested as a potential novel approach
293 to vaccine development by us and others (Burns, et al. 2009; Atkinson, et al. 2014; Gaunt, et al. 2016;

294 Moratorio, et al. 2017). Here we explore the evolutionary space occupied by coronaviruses in the
295 context of their CpG composition and find that SARS-CoV-2 has a low CpG composition in
296 comparison with other coronaviruses, but with CpG ‘hotspots’ in genomically disparate regions. This
297 highlights the potential for large scale recoding of the SARS-CoV-2 genome by introduction of CpGs
298 into multiple regions of the virus genome as a mechanism for generation of an attenuated live vaccine.
299 Introduction of CpG into multiple sites could also be used to subvert the potential of the virus to
300 revert to virulence through recombination. A challenge of live attenuated vaccine manufacture is to
301 enable sufficient production of a vaccine virus that has a replication defect. Strategic introduction of
302 CpGs into specific regions of the virus genome has the potential to negate a replication defect in ZAP
303 knockout cells, if regions such as conserved secondary structures and overlapping reading frames are
304 avoided (Ficarelli, et al. 2019; Odon, et al. 2019), thus allowing the generation of high titre
305 replication-defective vaccine virus stocks.

306

307 **Materials and Methods**

308 **Sequences.** For a comparison of GC content versus CpG ratio, all SARS-CoV-2 complete genome
309 sequences of high coverage (as defined on the GISAID website) were downloaded from GISAID
310 (www.gisaid.org) on 26 March 2020 (1163 sequences in total) and aligned against the SARS-COV-2
311 reference sequence (Accession number NC_045512) using Simmonics software (Simmonds 2012)
312 SSE v1.4 (pre-release download kindly provided by Prof. Peter Simmonds, Oxford University). All
313 sequences represented human isolates except for one sequence of bat origin (hCoV-
314 19/bat/Yunnan/RaTG13/2013; EPI_ISL_402131) and one sequence from a pangolin (hCoV-
315 19/pangolin/Guangdong/1/2019; EPI_ISL_410721). All complete genome sequences of all
316 coronaviruses were downloaded from NCBI on the 16 April 2020 (3407 sequences in total).
317 Sequences were then aligned and sequences less than 10% divergent at the nucleotide level, identified
318 using the ‘identify similar/ identical sequences’ function in SSE v1.4 were removed from the dataset.
319 Sequences were annotated into animal groups and genera based on their description in the NCBI
320 database. The trimmed dataset (**Table S1**) included 215 complete genome coronavirus sequences.
321 Individual groups were made for sequences originating from the following hosts: bat ($n = 108$), avian
322 (35), camelid (3), canine (7), feline (9), human (7), mustelids (5), rodents (8), swine (15), ungulates
323 (9) and ‘other’ (which included bottle-nosed dolphin (2), hedgehog (2), rabbit (2), beluga whale (1),
324 civet (1) and pangolin (1)). Groups were loosely defined based on taxonomic orders, with some
325 exceptions made to examine our specific research questions. Bats are of the order Chiroptera; multiple
326 avian orders were grouped together (Galliformes, Anseriformes, Passeriformes, Gruiformes,
327 Columbiformes and Pelicaniformes); even toed (Artiodactyla) and odd toed (Perissodactyla) ungulate
328 orders were grouped, with camelids analysed separately due to their association with MERS-CoV
329 (Azhar, et al. 2014); Canidae (canine) and Pantherinae (feline) sequences of the Carnivora order were
330 analysed separately, as canines have previously been suggested as an intermediate host species for
331 SARS-CoV-2 (Xia 2020) and cat infections with SARS-CoV-2 have been reported (Shi, et al. 2020);
332 humans were the only representatives from the Primate order; all remaining Carnivora, with the
333 exception of a single civet sequence, belonged to the Mustelidae (mustelids); rodents belong to the
334 Rodentia order; and swine belong to the Artiodactyla order; whales are also Artiodactyla but swine
335 were considered separately due to considerable interest in porcine coronaviruses (Vlasova, et al.
336 2020). Sequences were also annotated for genus by reference to the NCBI description (203 of the 215
337 sequences were assigned to a genus), and for primary replication site by literature reference (refer to
338 **Table S1**). Replication site annotations were based on the sample type from which a coronavirus
339 sequence was obtained – ‘enteric’ for faecal/ gastrointestinal samples, ‘respiratory’ for nasal,
340 oropharyngeal and other respiratory samples; ‘multiple’ if samples from multiple systems tested
341 positive, ‘other’ if the sample was collected from a site not falling into the enteric or respiratory
342 categories (e.g. brain), or ‘unknown’ if a sample type could not be determined. If only one sampling

343 route was tested and returned a positive result, the sequence was categorised in accordance with the
344 sole sampling route. The sequence datasets used in this paper are summarised in **Fig. 1**.

345 **Analyses of dinucleotide content.** CpG and UpA composition of complete genomes or of individual
346 ORFs were calculated using the composition scan in SSE v1.4. CpG frequencies were measured as
347 observed: expected (O:E) ratios, using the formula $f(\text{CpG})/f(\text{C}) \cdot f(\text{G})$. Individual ORFs were
348 identified using a combination of ORF finder (<https://www.ncbi.nlm.nih.gov/orffinder/>), visual
349 inspection of nucleotide alignments in SSE v1.4, comparison with previous literature and information
350 available from nextstrain.org. Sliding window analyses were performed on the 1163 aligned SARS-
351 CoV-2 sequences and the related bat and pangolin sequences by performing composition scans in SSE
352 v1.4 for 100 nucleotide genomic regions, at 25 nucleotide iterations. For the SARS-CoV-2 sequences,
353 mean CpG O:E ratios for each window were calculated. CPB (Gutman and Hatfield 1989) scores
354 across the SARS-CoV-2 ORFeome were calculated using the SSE v1.4 composition scan function.
355 Individual ORFs were concatenated with a separating 'NNN' codon for analysis, and secondary
356 overlapping ORFs were not included due to coding constraints imposed in these regions.

357 **Phylogenetic analyses.** E ORFs were aligned in MEGA X (Kumar, et al. 2018) using the Clustal
358 method. Of the 215 divergent sequences included in the analysis, E ORF could be identified in 178 by
359 homology with E ORFs previously annotated in NCBI. Of these 178 E ORFs, 7 were sequences
360 isolated from humans and 96 were from bats; these sequences were selected for analysis. Phylogenetic
361 reconstruction was performed using an unrooted maximum likelihood tree, with gamma distributed
362 variation in rates between branches and 100 bootstraps (also in MEGA X).

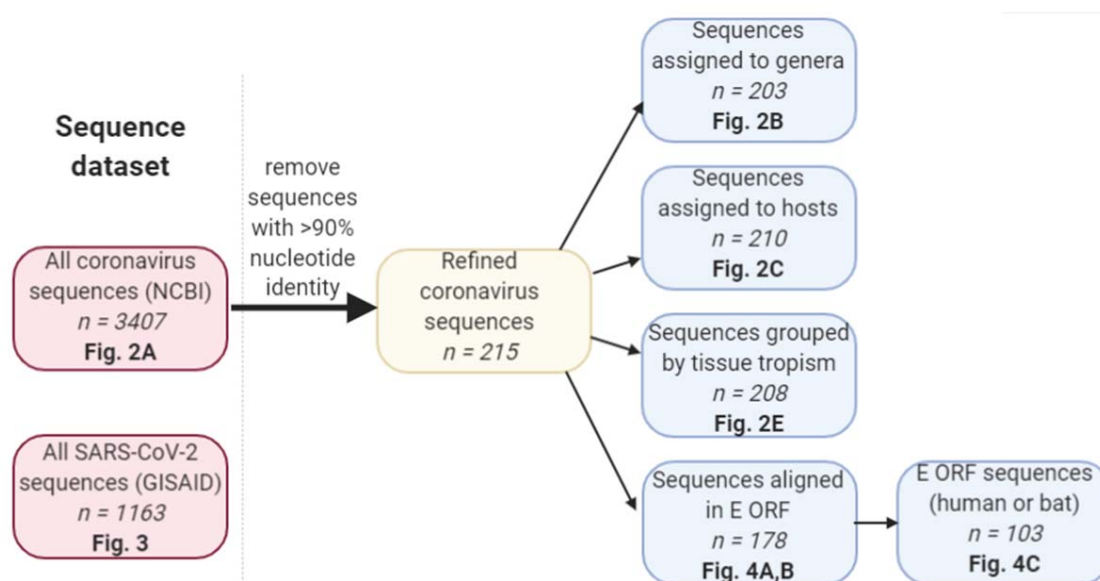
363 **Statistical analyses.** Comparison to determine whether there was a statistically significant difference
364 across groups was performed using a 1-way ANOVA in GraphPad Prism. Multi-way comparisons of
365 CpG composition between groups were performed using Tukey's multiple comparisons test in
366 GraphPad Prism. A 5% significance level was used throughout.

367

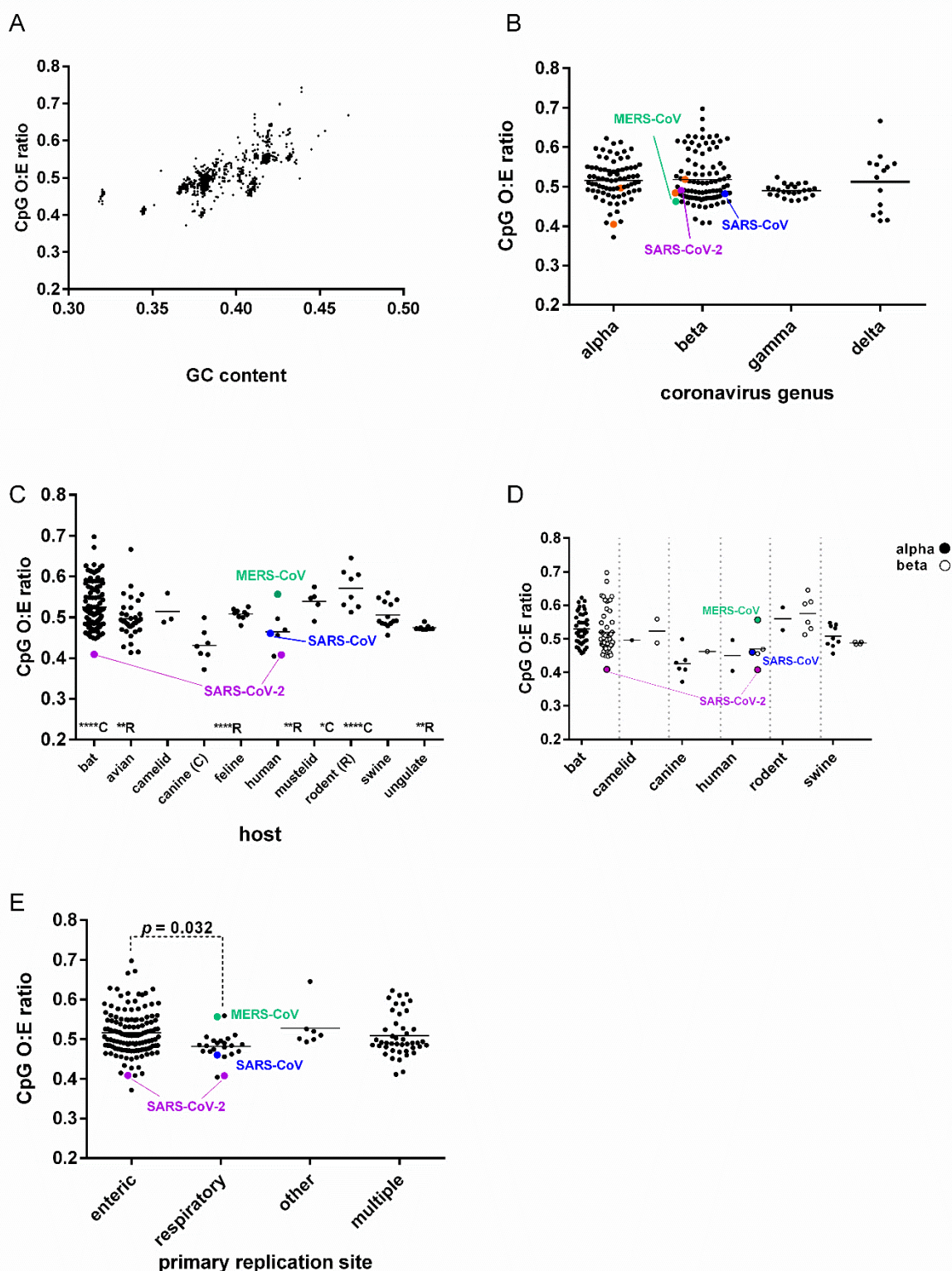
368 **Acknowledgements**

369 We would like to thank Prof. Peter Simmonds (Oxford University) for providing a pre-release version
370 of SSE v1.4. We are grateful to Dr James Glover (the Roslin Institute) for comments on the
371 manuscript. Figure 1 was created using BioRender. This work was supported by BBSRC Roslin
372 Institute Strategic Program Grant funding (no. BB/P013740/1 to PD and FG) and Wellcome Trust/
373 Royal Society Fellowship (211222/Z/18/Z to EG).

374 **Figures and legends.**



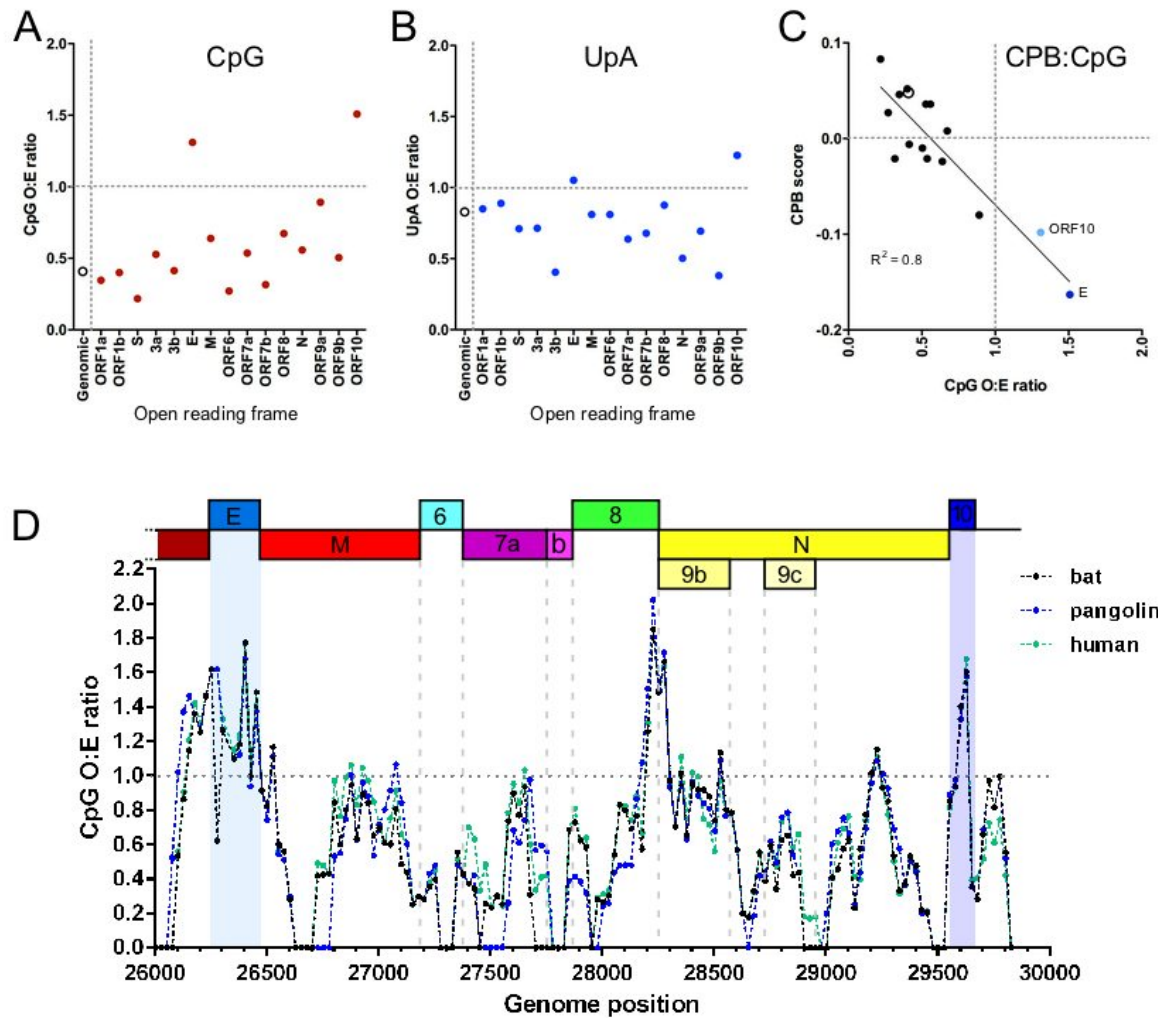
375
376 **Figure 1. Workflow for sequence processing.** Two sequence datasets were used for analysis; all
377 coronavirus complete genome sequences available on NCBI, and SARS-CoV-2 complete genome
378 sequences available on the GISAID platform (left hand pink shaded boxes). The coronavirus complete
379 genome sequences were cleaned by removal of sequences with 90% nucleotide identity or greater to
380 remove epidemiologic biases, leaving 215 complete genome sequences (central yellow shaded box).
381 These were then categorised by genera, host, and tissue tropism. The subset of 215 sequences were
382 also aligned over the E ORF and grouped by host (blue shaded boxes). Each box firstly describes each
383 dataset used, the number of sequences in that dataset is then indicated in *italicized* font, and the figure
384 to which the dataset corresponds is indicated in **bold** font.



385

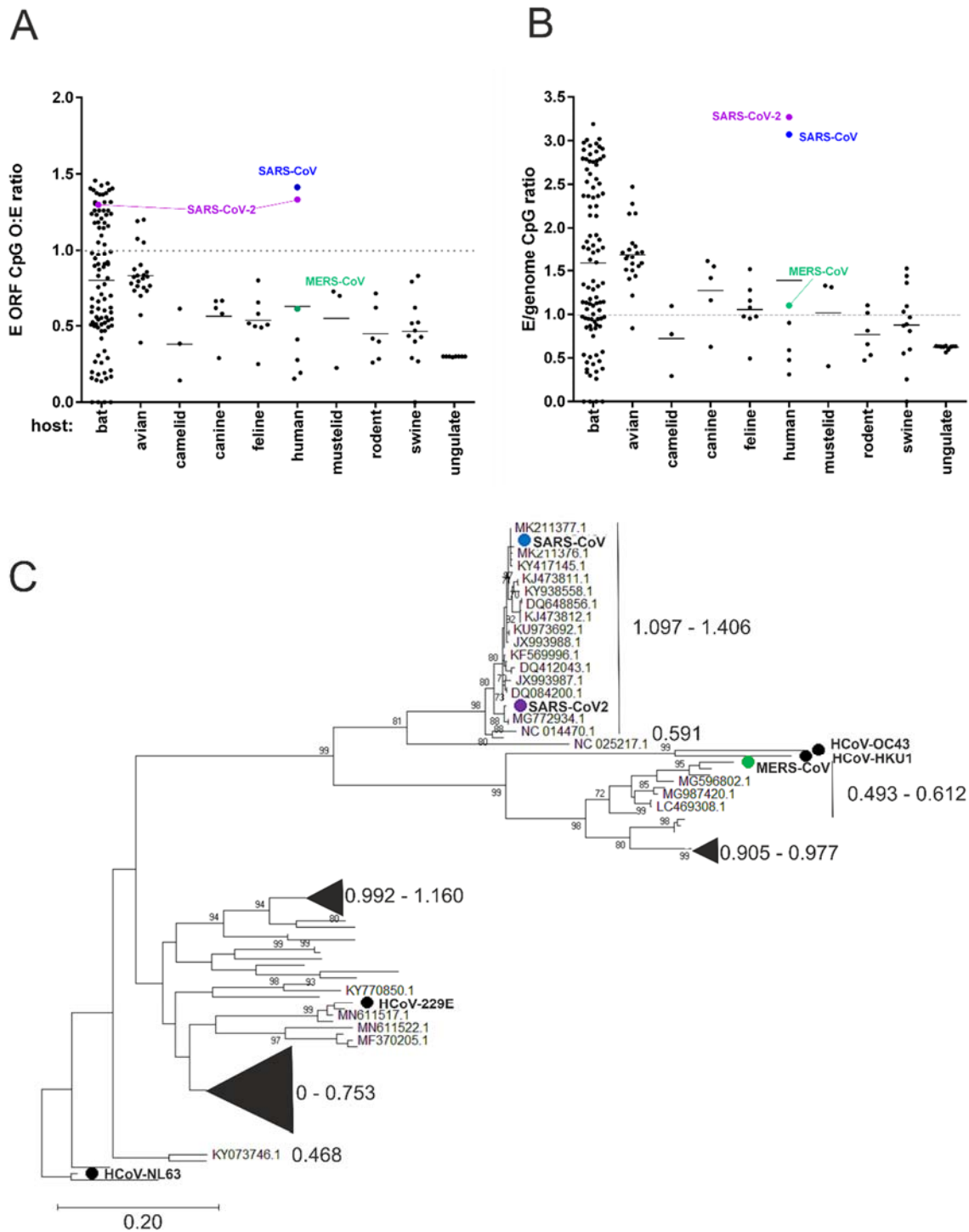
386 **Figure 2.** Comparison of the CpG ratios of complete genomes of coronaviruses. SARS-CoV is
 387 represented by a blue circle, SARS-CoV-2 by a purple circle and MERS-CoV by a green circle
 388 throughout. **A.** GC content versus CpG ratio for all complete genome sequences of coronaviruses
 389 downloaded from Genbank (3407 sequences). The sequence dataset in (A) was then stripped to
 390 include only one representative from sequences with less than 10% nucleotide diversity to overcome
 391 epidemiologic biases (215 representative sequences), which were analysed in the subsequent sub-

392 figures. **B.** Coronavirus genus against genomic CpG content. Other human-infecting coronaviruses
393 (HCoV-2292E, HCoV-NL63 (alphacoronaviruses) and HCoV-HKU1 and HCoV-OC43
394 (betacoronaviruses) are represented using orange circles. **C.** Vertebrate host of coronavirus against
395 genomic CpG content. Statistically significant differences between CpG compositions of viruses from
396 different hosts are indicated above the x axis line, with 'C' denoting a statistically significant
397 difference from canine coronaviruses and 'R' denoting a statistically significant difference from
398 rodent coronaviruses. Tukey's multiple comparisons test was used to identify differences in CpG
399 composition between viruses infecting different hosts. A p value < 0.05 is indicated with *, $p < 0.01 =$
400 **, $p < 0.001 =$ *** and $p < 0.0001 =$ ****. **D.** Vertebrate host of coronavirus, with further sub-
401 division into coronavirus genus, against genomic CpG content. Alphacoronaviruses are denoted with
402 filled circles and betacoronaviruses with open circles. **E.** Primary replication site against genomic
403 CpG content by host. Tukey's multiple comparisons test was used to identify differences in CpG
404 composition between viruses infecting different tissues. For a full breakdown of how these were
405 assigned, please refer to **Table S1**.



406

407 **Figure 3.** Heterogeneities in the dinucleotide composition of the SARS-CoV-2 genome. **A-C.**
 408 Comparison of the dinucleotide and coding compositions of SARS-CoV-2 open reading frames
 409 (ORFs) for **A.** CpG observed: expected (O:E) ratios, **B.** UpA O:E ratios and **C.** Codon pair bias (CPB)
 410 scores. Average scores across the genome are indicated using open circles. **D.** Sliding window
 411 analysis of CpG content of SARS-CoV-2 (green line) and closely related bat (black line) and pangolin
 412 (purple line) isolates. The CpG O:E ratio of the 3' end of the genome was measured in 100 nucleotide
 413 windows in 25 nucleotide increments. The mean of 1163 complete genome sequences is presented for
 414 SARS-CoV-2.



415

416 **Figure 4.** Evolutionary conservation of E ORF CpG content. MERS-CoV (green circle), SARS-CoV
 417 (blue circle) and SARS-CoV-2 (green circle) are indicated in both panels. **A.** Virus-dependent
 418 variation in E ORF CpG frequency. CpG O:E ratios for E ORF for 178 coronavirus E ORFs are
 419 plotted by host. **B.** CpG O:E ratios for E ORF were divided by the genomic CpG O:E ratio for 178
 420 coronavirus sequences and grouped by host. **C.** Phylogenetic reconstruction of E ORF of human and
 421 bat coronaviruses. Maximum composite likelihood tree (100 bootstraps) representing the seven
 422 human-infecting coronaviruses (HCoV-229E, HCoV-HKU1, HCoV-NL63, HCoV-OC43 (all black
 423 circles) and 96 bat coronaviruses for which E ORF could be identified by alignment with the human
 424 coronaviruses. CpG O:E ratios for the E gene are indicated by large font numbers, and the sequences

425 to which they relate are either bracketed or represented by triangles scaled to indicate the number of
426 sequences they represent.

427 **References**

428

429 Atkinson N, Witteveldt J, Evans D, Simmonds P. 2014. The influence of CpG and UpA dinucleotide
430 frequencies on RNA virus replication and characterization of the innate cellular pathways underlying
431 virus attenuation and enhanced replication. *Nucleic Acids Research* 42:4527-4545.

432 Azhar EI, El-Kafrawy SA, Farraj SA, Hassan AM, Al-Saeed MS, Hashem AM, Madani TA. 2014. Evidence
433 for Camel-to-Human Transmission of MERS Coronavirus. 370:2499-2505.

434 Banerjee A, Kulcsar K, Misra V, Frieman M, Mossman K. 2019. Bats and Coronaviruses. *Viruses* 11:41.

435 Berkhout B, van Hemert F. 2015. On the biased nucleotide composition of the human coronavirus
436 RNA genome. *Virus Research* 202:41-47.

437 Burns CC, Campagnoli R, Shaw J, Vincent A, Jorba J, Kew O. 2009. Genetic Inactivation of Poliovirus
438 Infectivity by Increasing the Frequencies of CpG and UpA Dinucleotides within and across
439 Synonymous Capsid Region Codons. 83:9957-9969.

440 Chenik M, Chebli K, Blondel D. 1995. Translation initiation at alternate in-frame AUG codons in the
441 rabies virus phosphoprotein mRNA is mediated by a ribosomal leaky scanning mechanism. 69:707-
442 712.

443 Cooper DN, Krawczak M. 1989. Cytosine methylation and the fate of CpG dinucleotides in vertebrate
444 genomes. *Human Genetics* 83:181-188.

445 Cotten M, Lam TT, Watson SJ, Palser AL, Petrova V, Grant P, Pybus OG, Rambaut A, Guan Y, Pillay D,
446 et al. 2013. Full-genome deep sequencing and phylogenetic analysis of novel human
447 betacoronavirus. *Emerging infectious diseases* 19:736-742B.

448 Cox E, Hooyberghs J, Pensaert MB. 1990. Sites of replication of a porcine respiratory coronavirus
449 related to transmissible gastroenteritis virus. *Research in veterinary science* 48:165-169.

450 Davidson A, Williamson MK, Lewis S, Shoemark D, Carroll M, Heesom K, Zambon M, Ellis J, Lewis P,
451 Hiscox J, et al. 2020. Characterisation of the transcriptome and proteome of SARS-CoV-2 using direct
452 RNA sequencing and tandem mass spectrometry reveals evidence for a cell passage induced in-
453 frame deletion in the spike glycoprotein that removes the furin-like cleavage site. In: bioRxiv.

454 Deaton AM, Bird A. 2011. CpG islands and the regulation of transcription. 25:1010-1022.

455 Dev RR, Ganji R, Singh SP, Mahalingam S, Banerjee S, Khosla S. 2017. Cytosine methylation by
456 DNMT2 facilitates stability and survival of HIV-1 RNA in the host cell during infection. *Biochemical*
457 *Journal* 474:2009-2026.

458 Ficarelli M, Wilson H, Pedro Galão R, Mazzon M, Antzin-Anduetza I, Marsh M, Neil SJD, Swanson CM.
459 2019. KHNYN is essential for the zinc finger antiviral protein (ZAP) to restrict HIV-1 containing
460 clustered CpG dinucleotides. *eLife* 8:e46767.

461 Firth AE, Atkins JF. 2010. Candidates in Astroviruses, Seadornaviruses, Cytorhabdoviruses and
462 Coronaviruses for +1 frame overlapping genes accessed by leaky scanning. *Virology Journal* 7:17.

463 Fitch B, Gorbatshevych O, Shen SH, Stauff CB, Song Y, Wang B, Leatherwood J, Gardin J, Yurovsky A,
464 Mueller S, et al. 2015. Reply to Simmonds et al.: Codon pair and dinucleotide bias have not been
465 functionally distinguished. 112:E3635-E3636.

466 Gaunt E, Wise HM, Zhang H, Lee LN, Atkinson NJ, Nicol MQ, Highton AJ, Klenerman P, Beard PM,
467 Dutia BM, et al. 2016. Elevation of CpG frequencies in influenza A genome attenuates pathogenicity
468 but enhances host response to infection. *eLife* 5:e12735-e12735.

469 Greenbaum BD, Levine AJ, Bhanot G, Rabadan R. 2008. Patterns of evolution and host gene mimicry
470 in influenza and other RNA viruses. *PLOS Pathogens* 4:e1000079-e1000079.

471 Groenke N, Trimpert J, Merz S, Conradie AM, Wyler E, Zhang H, Hazapis O-G, Rausch S, Landthaler
472 M, Osterrieder N, et al. 2020. Mechanism of Virus Attenuation by Codon Pair Deoptimization. *Cell*
473 *Reports* 31:107586.

474 Guo X, Ma J, Sun J, Gao G. 2007. The zinc-finger antiviral protein recruits the RNA processing
475 exosome to degrade the target mRNA. 104:151-156.

- 476 Gutman GA, Hatfield GW. 1989. Nonrandom utilization of codon pairs in *Escherichia coli*. 86:3699-
477 3703.
- 478 Hiscott J, Kwon H, Génin P. 2001. Hostile takeovers: viral appropriation of the NF- κ B pathway. *The*
479 *Journal of Clinical Investigation* 107:143-151.
- 480 Hu B, Ge X, Wang L-F, Shi Z. 2015. Bat origin of human coronaviruses. *Virology Journal* 12:221.
- 481 Irigoyen N, Firth AE, Jones JD, Chung BYW, Siddell SG, Brierley I. 2016. High-Resolution Analysis of
482 Coronavirus Gene Expression by RNA Sequencing and Ribosome Profiling. *PLOS Pathogens*
483 12:e1005473-e1005473.
- 484 Kanaya S, Yamada Y, Kinouchi M, Kudo Y, Ikemura T. 2001. Codon Usage and tRNA Genes in
485 Eukaryotes: Correlation of Codon Usage Diversity with Translation Efficiency and with CG-
486 Dinucleotide Usage as Assessed by Multivariate Analysis. *Journal of Molecular Evolution* 53:290-298.
- 487 Khoddami V, Cairns BR. 2013. Identification of direct targets and modified bases of RNA cytosine
488 methyltransferases. *Nature Biotechnology* 31:458-464.
- 489 Kim D, Lee J-Y, Yang J-S, Kim JW, Kim VN, Chang H. 2020. The architecture of SARS-CoV-2
490 transcriptome.2020.2003.2012.988865.
- 491 Kozak M. 1986. Point mutations define a sequence flanking the AUG initiator codon that modulates
492 translation by eukaryotic ribosomes. *Cell* 44:283-292.
- 493 Kumar S, Stecher G, Li M, Knyaz C, Tamura K. 2018. MEGA X: Molecular Evolutionary Genetics
494 Analysis across Computing Platforms. *Molecular Biology and Evolution* 35:1547-1549.
- 495 Kunec D, Osterrieder N. 2016. Codon Pair Bias Is a Direct Consequence of Dinucleotide Bias. *Cell*
496 *Reports* 14:55-67.
- 497 Liao CL, Lai MM. 1994. Requirement of the 5'-end genomic sequence as an upstream cis-acting
498 element for coronavirus subgenomic mRNA transcription. 68:4727-4737.
- 499 Lin C-G, Lo SJ. 1992. Evidence for involvement of a ribosomal leaky scanning mechanism in the
500 translation of the hepatitis B virus Pol gene from the viral pregenome RNA. *Virology* 188:342-352.
- 501 Lin Y-T, Chiweshe S, McCormick D, Raper A, Wickenhagen A, DeFillipis V, Gaunt E, Simmonds P,
502 Wilson SJ, Grey F. 2020. Human cytomegalovirus evades ZAP detection by suppressing CpG
503 dinucleotides in the major immediate early genes.2020.2001.2007.897132.
- 504 Lu R, Zhao X, Li J, Niu P, Yang B, Wu H, Wang W, Song H, Huang B, Zhu N, et al. 2020. Genomic
505 characterisation and epidemiology of 2019 novel coronavirus: implications for virus origins and
506 receptor binding. *The Lancet* 395:565-574.
- 507 Marra MA, Jones SJM, Astell CR, Holt RA, Brooks-Wilson A, Butterfield YSN, Khattra J, Asano JK,
508 Barber SA, Chan SY, et al. 2003. The Genome Sequence of the SARS-Associated Coronavirus.
509 300:1399-1404.
- 510 McClelland M, Ivarie R. 1982. Asymmetrical distribution of CpG in an 'average' mammalian gene.
511 *Nucleic Acids Research* 10:7865-7877.
- 512 Medvedeva YA, Khamis AM, Kulakovskiy IV, Ba-Alawi W, Bhuyan MSI, Kawaji H, Lassmann T, Harbers
513 M, Forrest ARR, Bajic VB, et al. 2014. Effects of cytosine methylation on transcription factor binding
514 sites. *BMC Genomics* 15:119.
- 515 Moratorio G, Henningsson R, Barbezange C, Carrau L, Bordería AV, Blanc H, Beaucourt S, Poirier EZ,
516 Vallet T, Boussier J, et al. 2017. Attenuation of RNA viruses by redirecting their evolution in sequence
517 space. *Nature Microbiology* 2:17088.
- 518 O'Connor JB, Brian DA. 2000. Downstream Ribosomal Entry for Translation of Coronavirus TGEV
519 Gene 3b. *Virology* 269:172-182.
- 520 Odon V, Fros JJ, Goonawardane N, Dietrich I, Ibrahim A, Alshaihahmed K, Nguyen D, Simmonds P.
521 2019. The role of ZAP and OAS3/RNaseL pathways in the attenuation of an RNA virus with elevated
522 frequencies of CpG and UpA dinucleotides. *Nucleic Acids Research* 47:8061-8083.
- 523 Perlman S, Netland J. 2009. Coronaviruses post-SARS: update on replication and pathogenesis.
524 *Nature Reviews Microbiology* 7:439-450.
- 525 Rasschaert D, Duarte M, Laude H. 1990. Porcine respiratory coronavirus differs from transmissible
526 gastroenteritis virus by a few genomic deletions. 71:2599-2607.

- 527 Rima BK, McFerran NV. 1997. Dinucleotide and stop codon frequencies in single-stranded RNA
528 viruses. 78:2859-2870.
- 529 Rota PA, Oberste MS, Monroe SS, Nix WA, Campagnoli R, Icenogle JP, Peñaranda S, Bankamp B,
530 Maher K, Chen M-h, et al. 2003. Characterization of a Novel Coronavirus Associated with Severe
531 Acute Respiratory Syndrome. 300:1394-1399.
- 532 Ryabova LA, Pooggin MM, Hohn T. 2006. Translation reinitiation and leaky scanning in plant viruses.
533 Virus Research 119:52-62.
- 534 Sawicki SG, Sawicki DL. 1998. A New Model for Coronavirus Transcription. In: Enjuanes L, Siddell SG,
535 Spaan W, editors. Coronaviruses and Arteriviruses. Boston, MA: Springer US. p. 215-219.
- 536 Sawicki SG, Sawicki DL, Siddell SG. 2007. A Contemporary View of Coronavirus Transcription. 81:20-
537 29.
- 538 Schaecher SR, Mackenzie JM, Pekosz A. 2007. The ORF7b Protein of Severe Acute Respiratory
539 Syndrome Coronavirus (SARS-CoV) Is Expressed in Virus-Infected Cells and Incorporated into SARS-
540 CoV Particles. 81:718-731.
- 541 Schneider PA, Kim R, Lipkin WI. 1997. Evidence for translation of the Borna disease virus G protein by
542 leaky ribosomal scanning and ribosomal reinitiation. 71:5614-5619.
- 543 Senanayake SD, Brian DA. 1997. Bovine coronavirus I protein synthesis follows ribosomal scanning
544 on the bicistronic N mRNA. Virus Research 48:101-105.
- 545 Shi J, Wen Z, Zhong G, Yang H, Wang C, Huang B, Liu R, He X, Shuai L, Sun Z, et al. 2020. Susceptibility
546 of ferrets, cats, dogs, and other domesticated animals to SARS–coronavirus 2.eabb7015.
- 547 Simmonds P. 2012. SSE: a nucleotide and amino acid sequence analysis platform. BMC Research
548 Notes 5:50.
- 549 Simmonds P, Xia W, Baillie JK, McKinnon K. 2013. Modelling mutational and selection pressures on
550 dinucleotides in eukaryotic phyla –selection against CpG and UpA in cytoplasmically expressed RNA
551 and in RNA viruses. BMC Genomics 14:610.
- 552 Squires JE, Patel HR, Nusch M, Sibbritt T, Humphreys DT, Parker BJ, Suter CM, Preiss T. 2012.
553 Widespread occurrence of 5-methylcytosine in human coding and non-coding RNA. Nucleic Acids
554 Research 40:5023-5033.
- 555 Sved J, Bird A. 1990. The expected equilibrium of the CpG dinucleotide in vertebrate genomes under
556 a mutation model. 87:4692-4696.
- 557 Takata MA, Gonçalves-Carneiro D, Zang TM, Soll SJ, York A, Blanco-Melo D, Bieniasz PD. 2017. CG
558 dinucleotide suppression enables antiviral defence targeting non-self RNA. Nature 550:124-127.
- 559 Tang Q, Wang X, Gao G. 2017. The Short Form of the Zinc Finger Antiviral Protein Inhibits Influenza A
560 Virus Protein Expression and Is Antagonized by the Virus-Encoded NS1. 91:e01909-01916.
- 561 Tats A, Tenson T, Remm M. 2008. Preferred and avoided codon pairs in three domains of life. BMC
562 Genomics 9:463.
- 563 Tomso DJ, Bell DA. 2003. Sequence Context at Human Single Nucleotide Polymorphisms:
564 Overrepresentation of CpG Dinucleotide at Polymorphic Sites and Suppression of Variation in CpG
565 Islands. Journal of Molecular Biology 327:303-308.
- 566 Tulloch F, Atkinson NJ, Evans DJ, Ryan MD, Simmonds P. 2014. RNA virus attenuation by codon pair
567 deoptimisation is an artefact of increases in CpG/UpA dinucleotide frequencies. eLife 3:e04531.
- 568 van der Hoek L, Pyrc K, Jebbink MF, Vermeulen-Oost W, Berkhout RJM, Wolthers KC, Wertheim-van
569 Dillen PME, Kaandorp J, Spaargaren J, Berkhout B. 2004. Identification of a new human coronavirus.
570 Nature Medicine 10:368-373.
- 571 Vlasova AN, Wang Q, Jung K, Langel SN, Malik YS, Saif LJ. 2020. Porcine Coronaviruses. Emerging and
572 Transboundary Animal Viruses:79-110.
- 573 Wise HM, Barbezange C, Jagger BW, Dalton RM, Gog JR, Curran MD, Taubenberger JK, Anderson EC,
574 Digard P. 2011. Overlapping signals for translational regulation and packaging of influenza A virus
575 segment 2. Nucleic Acids Research 39:7775-7790.

576 Woo PCY, Lau SKP, Chu C-m, Chan K-h, Tsoi H-w, Huang Y, Wong BHL, Poon RWS, Cai JJ, Luk W-k, et
577 al. 2005. Characterization and Complete Genome Sequence of a Novel Coronavirus, Coronavirus
578 HKU1, from Patients with Pneumonia. 79:884-895.
579 Woo PCY, Wong BHL, Huang Y, Lau SKP, Yuen K-Y. 2007. Cytosine deamination and selection of CpG
580 suppressed clones are the two major independent biological forces that shape codon usage bias in
581 coronaviruses. *Virology* 369:431-442.
582 Xia X. 2020. Extreme genomic CpG deficiency in SARS-CoV-2 and evasion of host antiviral defense.
583 *Molecular Biology and Evolution*.
584 Xie L, Lu B, Zheng Z, Miao Y, Liu Y, Zhang Y, Zheng C, Ke X, Hu Q, Wang H. 2018. The 3C protease of
585 enterovirus A71 counteracts the activity of host zinc-finger antiviral protein (ZAP). 99:73-85.
586 Zaki AM, van Boheemen S, Bestebroer TM, Osterhaus ADME, Fouchier RAM. 2012. Isolation of a
587 Novel Coronavirus from a Man with Pneumonia in Saudi Arabia. 367:1814-1820.
588 Zhu N, Zhang D, Wang W, Li X, Yang B, Song J, Zhao X, Huang B, Shi W, Lu R, et al. 2020. A Novel
589 Coronavirus from Patients with Pneumonia in China, 2019. *New England Journal of Medicine*
590 382:727-733.

591